Modern Krylov Subspace Methods in Electromagnetic Field Computation Using the Finite Integration Theory

MARKUS CLEMENS, ROLF SCHUHMANN, URSULA VAN RIENEN and THOMAS WEILAND
Fachbereich 18 Elektrische Nachrichtentechnik, Fachgebiet Theorie Elektromagnetischer Felder
Technische Hochschule Darmstadt, Schloßgartenstrasse 8, D-64289 Darmstadt, Germany
clemen@temf00.temf.e-technik.th-darmstadt.de
dd80 (Schuhmann), dd6c (van Rienen), dd2e (Weiland) @ same location

Abstract

A theoretical basis for numerical electromagnetics, the so-called Finite Integration Theory, is described. Based upon Maxwell's equations in their integral form, it results in a set of matrix equations, each of which is a discrete analogue of its original analytical equation. Applications of this discretization process are described here in the context of the numerical simulation of electroquasistatic problems and of time-harmonic field computations including a new type of waveguide boundary condition, which is presented here for the first time. In both fields the process of mathematical modelling and discretization yields large systems of complex linear equations which have to be solved numerically. For this task several modern Krylov subspace methods are presented such as BiCG, CGS and their more recent stabilized variants CGS2, BiCGSTAB(l) and TFQMR. They are applied in connection with efficient preconditioning methods. The applicability of these modern methods is shown for a number of examples for both problem types.

1 Introduction

A well-known discretization approach in the computation of electromagnetic fields is the so-called Finite Integration Theory (FIT). FIT and the related software were originally developed for frequency domain applications [29], [30], [31] and later for solving many different problems including static, low frequency, high frequency and transient fields for designing large scale accelerators [32].

In the following we will give short overview on the basic ideas of FIT. In order to avoid the restriction to coordinate grids and to improve the capability of a grid to approximate curved boundaries, we will present a generalized form of the discretization approach, which is applicable even to non-coordinate grids having the following properties. One can define a general grid doublet $\{\mathbf{G} - \tilde{\mathbf{G}}\}$:

- The solution volume $\mathbf{G}$ is simply connected and contained in R^3 (or R^2).
- $\mathbf{G}$ is a finite set of non-empty sub-volumes:

$$\mathbf{V} = \{V_1 \dots V_{n_V}\};\ \cap V_i = \{A_i\};\ \cup V_i = \mathbf{G}$$

- The non-empty areas A_i are defined as the intersections of two volumes:

$$\mathbf{A} = \{A_1 \dots A_{n_A}\} \text{ with } \{A_i\} := \cap V_i,$$

- Lines L_i are defined by the intersection of areas:

$$\mathbf{L} = \{L_1 \dots L_{n_L}\} \text{ with } \{L_i\} := \cap A_i,$$

- Points P_i are defined by the intersections of lines:

$$\mathbf{P} = \{P_1 \dots P_{n_P}\} \text{ with } \{P_i\} := \cap L_i, .$$

On such a grid $\mathbf{G}$ it is more convenient to use integrated fields as state variables rather than the field components directly.

If we define a grid *voltage* along a grid line L_i and a magnetic flux quantity by:

$$e_i = \int_{L_i} \vec{E} \cdot d\vec{s}\ ;\ b_i = \int_{A_i} \vec{B} \cdot d\vec{A} \tag{1}$$

we can rewrite the first Maxwell equation on $\mathbf{G}$:

$$\oint \vec{E} \cdot \vec{ds} = -\int \frac{\partial \vec{B}}{\partial t} \cdot \vec{dA} \tag{2}$$

in *exact* representation as:

$$\sum_k c_{ik} e_k = -\frac{\partial b_i}{\partial t}. \tag{3}$$

The coefficients $c_{i,k}$ build a $3N \times 3N$ matrix $\mathbf{C}$ (N = number of grid points), consisting only of the entries

$\{-1, 0, 1\}$. This matrix can be considered to be the discrete analogue of the analytical **curl**-operator.

So far no approximation and no discretization is applied. The only step from the original field equation to the latter one was to replace field components by their exact integrals along lines or over areas.

Similarly we continue with replacing the second Maxwell equation but on $\tilde{\mathbf{G}}$ rather than on $\mathbf{G}$, where $\tilde{\mathbf{G}}$ is defined such that each point $\tilde{P}_i$ of $\tilde{\mathbf{G}}$ is located inside V_i of $\mathbf{G}$. On this dual grid $\tilde{\mathbf{G}} = \{\tilde{V}_{nv}\}$ we introduce magnetic voltages h_i, electric fluxes d_i and currents j_i as:

$$h_i = \int_{\tilde{L}_i} \vec{H} \cdot d\vec{s} \; ; \; , d_i = \int_{\tilde{A}_i} \vec{D} \cdot d\vec{A} \; ; \; j_i = \int_{\tilde{A}_i} \vec{J} \cdot d\vec{A} \quad (4)$$

As an example Fig. 1 shows the allocation of the state variables on an orthogonal cartesian grid doublet.

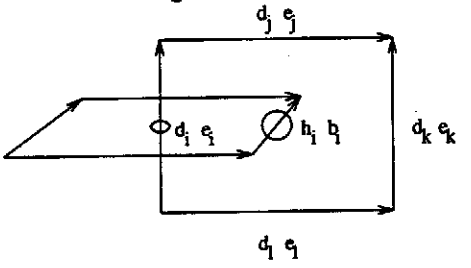

Figure 1: One cell of the grid $\mathbf{G}$ and the dual grid $\tilde{\mathbf{G}}$. The allocation of the electric field and flux components are shown as well as the allocations of the corresponding magnetic quantities.

With these new variables we can again map the original equation

$$\oint \vec{H} \cdot \vec{ds} = \int (\frac{\partial \vec{D}}{\partial t} + \vec{J}) \cdot \vec{dA} \quad (5)$$

to a grid equation exactly:

$$\sum_k \tilde{c}_{ik} h_k = \frac{\partial d_i}{\partial t} + j_i. \quad (6)$$

The third and fourth Maxwell equation is similarly transformed into

$$\sum_k \tilde{s}_{ik} d_k = q_i \; ; \; \sum_k s_{ik} b_k = 0 \; ; \text{ with } q_i = \int_{V_i} \rho \, dV, \quad (7)$$

where the coefficients $\tilde{c}_{ik}, \tilde{s}_{ik}$ and s_{ik} again build topological matrices $\tilde{\mathbf{C}}, \tilde{\mathbf{S}}$ and $\mathbf{S}$.

So far we have mapped all Maxwell equations to a grid space doublet without any specialization. The final discretization comes into the procedure only now that we have to relate electric voltages and fluxes, and magnetic voltages and fluxes as well. In the above derivation the magnetic voltage and the magnetic flux are independent variables. The relation f must be of the form:

$$f(\vec{B}, \vec{H}) = \frac{\int_{A_i} \vec{B} \cdot d\vec{A}}{\int_{\tilde{L}_i} \vec{H} \cdot d\vec{s}} \approx D_{\mu,i}$$

The matrix $\mathbf{D}_\mu$ is now the discrete representation of the permeability. Thus in this derivation the approximation is introduced through the material relations rather than difference expressions for derivatives.

In general this matrix is not diagonal but sparse with some diagonals of non-zero elements. Furthermore $\mathbf{D}_\mu$ is symmetric for reciprocal materials. In the case of coordinate grids as well as for a few other orthogonal grid doublets (cf. [28]) the discretization of the material equation has a second order accuracy **and** the material matrices are truly diagonal if the material tensors are diagonal or isotropic.

The same arguments lead to the discrete permittivity and conductivity as (in general not diagonal) matrices:

$$\mathbf{d} = \mathbf{D}_\epsilon \mathbf{e} \; ; \; \mathbf{j} = \mathbf{D}_\kappa \mathbf{e} \quad (8)$$

Summarizing this derivation yields the so-called Maxwell Grid Equations (MGE), corresponding *one-to-one* to the analytical equations on any non-regular grid doublet obeying the above definitions.

Integral Form:

$$\begin{aligned}
\iint_A -\frac{\partial}{\partial t} \vec{B} \cdot d\vec{A} &= \oint_{\partial A} \vec{E} \cdot d\vec{r} \quad (9)\\
\iint_{\partial V} \vec{B} \cdot d\vec{A} &= 0\\
\iint_{\tilde{A}} \left(\vec{J} + \frac{\partial}{\partial t} \vec{D} \right) \cdot d\vec{\tilde{A}} &= \oint_{\partial \tilde{A}} \vec{H} \cdot d\vec{\tilde{r}}\\
\int_{\partial \tilde{V}} \vec{D} \cdot d\vec{\tilde{A}} &= \iiint_{\tilde{V}} \varrho \, d\tilde{V}\\
\vec{D} &= \epsilon \vec{E}\\
\vec{B} &= \mu \vec{H}\\
\vec{J}_L &= \kappa \vec{E}
\end{aligned}$$

Matrix Representation:

$$\begin{aligned}
-\dot{\mathbf{b}} &= \mathbf{C}\,\mathbf{e}\\
\mathbf{S}\,\mathbf{b} &= \mathbf{0}\\
\mathbf{j} + \dot{\mathbf{d}} &= \tilde{\mathbf{C}}\,\mathbf{h}\\
\tilde{\mathbf{S}}\,\mathbf{d} &= \mathbf{q}\\
\mathbf{d} &= \mathbf{D}_\epsilon\,\mathbf{e}\\
\mathbf{b} &= \mathbf{D}_\mu\,\mathbf{h}\\
\mathbf{j}_L &= \mathbf{D}_\kappa\,\mathbf{e}
\end{aligned}$$

So far this theory is state of the art and the basis for existing computer codes solving problems in time domain, frequency domain and in statics [14].

It represents the only known theory that not only allows practical solution on a computer but also maintains all analytical properties of the electromagnetic fields when changing from R^3 to the grid space.

1.1 Algebraic Properties of Maxwell's Grid Equations

Grid-fields, as obtained by FIT, have analytical and algebraic properties that ensure accurate numerical results and enable an algebraically exact, self-testing of numerical results.

These properties may be considered useful in two ways. One aspect is that many numerical problems are a priori eliminated, such as spurious modes and parasitic charges.

Another aspect is that the matrix theory can be used instead of the analytical equations to study properties of fields in an algebraic manner, without actually solving the equations numerically.

For grid doublets there exists a dual index system such that the point $\tilde{P}_i$ is located inside V_i and, vice versa, P_i inside $\tilde{V}_i$. All other elements of $\mathbf{G}, \tilde{\mathbf{G}}$ receive an index defined by this system as well. This numbering scheme ensures that the following key properties hold [33], [5], [10], [4]:

$$\mathbf{C} = \tilde{\mathbf{C}}^{\mathbf{T}} \tag{10}$$

$$\mathbf{S}\,\mathbf{C} = \mathbf{0} \tag{11}$$

Both equations represent a topological property resulting from the duality of the two grids. The analytical and algebraic properties resulting from these basic equations are [33]:

$$\mathbf{C}\,\mathbf{S} = \mathbf{0} \;\leftrightarrow\; \mathbf{curl\,grad} = \mathbf{0} \tag{12}$$

$$\mathbf{S}\,\mathbf{C} = \mathbf{0} \;\leftrightarrow\; \mathbf{div\,curl} = \mathbf{0} \tag{13}$$

and similarly for the dual grid operators:

$$\tilde{\mathbf{C}}\,\tilde{\mathbf{S}} = \mathbf{0} \;\leftrightarrow\; \mathbf{curl\,grad} = \mathbf{0} \tag{14}$$

$$\tilde{\mathbf{S}}\,\tilde{\mathbf{C}} = \mathbf{0} \;\leftrightarrow\; \mathbf{div\,curl} = \mathbf{0} \tag{15}$$

As an example for a proof using algebra we consider the (well known) fact, that resonant fields in loss free structures can have only real eigenfrequencies. For the case of MGE it requires only a few lines to prove this. We rewrite the MGE in frequency domain as:

$$\mathbf{Ce} = -i\omega\mathbf{b} \tag{16}$$

$$\tilde{\mathbf{C}}\mathbf{D}_\mu^{-1}\mathbf{b} = +i\omega\mathbf{D}_\epsilon\mathbf{e} \tag{17}$$

We combine both equations to

$$\tilde{\mathbf{C}}\mathbf{D}_\mu^{-1}\mathbf{Ce} = \omega^2\mathbf{D}_\epsilon\mathbf{e}, \tag{18}$$

introduce an energy density normalization by

$$\tilde{\mathbf{e}} = \mathbf{D}_\epsilon^{1/2}\,\mathbf{e} \tag{19}$$

and finally obtain:

$$(\mathbf{D}_\epsilon^{-1/2}\tilde{\mathbf{C}}\mathbf{D}_\mu^{-1/2})\,(\mathbf{D}_\epsilon^{-1/2}\tilde{\mathbf{C}}\mathbf{D}_\mu^{-1/2})^{\mathbf{T}}\,\tilde{\mathbf{e}} = \omega^2\,\tilde{\mathbf{e}} \tag{20}$$

This equation is a simple, algebraic, linear eigenvalue problem with an (obviously) symmetric and real matrix of the form A^TA. Thus one knows from the algebra that all eigenvalues ω^2 are real and non-negative, q.e.d.

To prove another very important property we start again from the eigenvalue equation (18) and multiply it from the left with $\tilde{\mathbf{S}}$:

$$\tilde{\mathbf{S}}\tilde{\mathbf{C}}\mathbf{D}_\mu^{-1}\mathbf{Ce} = \omega^2\tilde{\mathbf{S}}\mathbf{D}_\epsilon\mathbf{e} \tag{21}$$

As the left hand side vanishes due to $\tilde{\mathbf{S}}\tilde{\mathbf{C}} = \mathbf{0}$ we are left with:

$$0 = \omega^2\tilde{\mathbf{S}}\mathbf{D}_\epsilon\mathbf{e} \tag{22}$$

This equation allows only two distinct cases for the solutions { e,d } :

$$\mathbf{e},\mathbf{d}: \begin{cases} \omega^2 = 0 & \tilde{\mathbf{S}}\mathbf{d} \neq \mathbf{0} \\ \omega^2 \neq 0 & \tilde{\mathbf{S}}\mathbf{d} = \mathbf{0} \end{cases}$$

As the original eigenvalue problem is real and symmetric we can create a set of orthonormal eigenmodes $\mathbf{e_n}$ such that

$$\mathbf{e_i^T e_j} = \delta_{\mathbf{ij}} \tag{23}$$

Thus the solution space Ω of equation (20) is made of two orthogonal sub spaces:

$$\Omega = \Omega_0 \oplus \Omega_\omega \tag{24}$$

This relation is in so far essential as one is only interested in solutions of Ω_ω and not in static fields contained in Ω_0. However, as the eigenvalue problem contains both solutions, this fact is also responsible for a significant problem: for N grid nodes there are approximately N zero and $2N$ non-zero eigenvalues. This almost excludes a numerical approach with iterative methods as it is almost impossible for large N to compute the $N+1$ th eigenvalue and vector. The solution to this problem is found by transforming the eigenvalue equation (18)into a discrete Helmholtz-like equation in analogy to the analytical step:

$$\mathbf{curl\,curl} = \mathbf{grad\,div} - \nabla^2 \tag{25}$$

This transition to ∇^2 is not possible in a one-to-one manner as it implies a constant material property function. Thus a similar transition with MGE will be more general as there is no restriction to constant material properties. The generalized Helmholtz-Grid-Equation reads as [33] [10]:

$$(\tilde{\mathbf{C}}\mathbf{D}_{\mu}^{-1}\mathbf{C} + \mathbf{D}_1\tilde{\mathbf{S}}^{\mathbf{T}}\mathbf{D}_2\tilde{\mathbf{S}}\mathbf{D}_3)\mathbf{e} = \omega^2\mathbf{e} \qquad (26)$$

where the term $\mathbf{D}_1\tilde{\mathbf{S}}^{\mathbf{T}}\mathbf{D}_2\tilde{\mathbf{S}}\mathbf{D}_3$ corresponds to the **grad-div** operator and $\mathbf{D}_1, \mathbf{D}_2, \mathbf{D}_3$ are diagonal matrices which can be constructed in such a way that the Helmholtz-Grid-Equation in homogeneous regions turns into the standard discretization of the ∇^2 operator. However, this form is valid for any non-constant material distribution. This is one of the rare cases where the grid equation is more general than the commonly used analytical one.

The solution space $\Omega_{\nabla 2}$ is again a set of two distinct orthogonal sub spaces:

$$\Omega_{\nabla 2} = \Omega_\gamma \oplus \Omega_\omega \qquad (27)$$

where the Ω_ω has not been altered. All static solutions with eigenvalue zero in Ω_0 are turned into eigensolutions of

$$\mathbf{D}_1\tilde{\mathbf{S}}^{\mathbf{T}}\mathbf{D}_2\tilde{\mathbf{S}}\mathbf{D}_3\mathbf{e} = \omega^2\mathbf{D}_\epsilon\mathbf{e} \qquad (28)$$

These eigenmodes are **not** solutions of Maxwell's equations. However, the advantadge of this transformation is that the eigenvalues of Ω_γ are also positive and real. The disadvantadge on the other hand is that these solutions are naturally obtained together with Maxwellian solutions. Historically these solutions were probably first observed by simply discretizing the wave equation with a conventional 6-star operator and investigating the fields obtained. As solutions in Ω_γ can often be identified by a trained user as non-Maxwellian, they were named *ghost* modes, *spurious* modes or simply *unphysical* solutions. With the exact relations shown above this *contamination* can be taken care of exactly within the MGE. Thus the widespread problem of *spurious modes*, which are subject to enormous effort in e.g. Finite Element studies, is simply a non-problem for MGE [29] [30] [31] [33].

Incidentally, for the reader interested in physics beyond Maxwell's equations, the solutions in Ω_γ are **not at all** unphysical. It is true that they are not electromagnetic solutions but they are in fact solutions of the Schroedinger equation.

2 Electro-Quasistatics

The practical background of the electro-quasistatics originates in energy engineering. An important problem in high-tension power plants are arc-overs on moist or contaminated insulators. The electrostatic field of the charge-free space prevails essentially below a critical voltage U_k. However, the dielectric material loses its insulating characteristics above U_k. It becomes the carrier of a discharge which builds up a conducting connection along the insulator. It is caused by slowly varying fields (50 Hz), for which the displacement current is a significant quantity. This class of problems is denoted as electro-quasistatics. The electro-quasistatic fields can be determined by solving a complex potential problem. Discretization leads to a large sparse system of complex linear equations with a symmetric matrix.

As a typical application, high voltage devices, which are driven with 50 Hz a.c. voltage, have been studied. There exists a voltage dependant electric source field $\vec{E}_Q$ and an a.c. current with density $\partial\vec{D}/\partial t$. This a.c. current is linked with a time dependent magnetic field which, in turn, causes an electric rotational field $\vec{E}_W$ with density $\mathrm{curl}\,\vec{E}_W = -\partial\vec{B}/\partial t$. The importance of this eddy field is determined by the rate of magnetic field variation. This rate is so low for 50 Hz that the local contribution of the eddy field strength is negligible compared to the source field strength.

2.1 Modelling

As a subject one considers lamellar, low frequency fields with important effects by the displacement current. Thus

$$\frac{\partial\vec{\mathbf{B}}}{\partial t} = \mathbf{0}, \frac{\partial\vec{\mathbf{D}}}{\partial t} \neq \mathbf{0} \qquad (29)$$

is assumed. Under these assumptions Maxwell's equations for the time harmonic electromagnetic field reduce to

$$\mathbf{curl}\,\underline{\vec{\mathbf{E}}} = \mathbf{0} \qquad (30)$$

$$\mathbf{curl}\,\underline{\vec{\mathbf{H}}} = i\omega\underline{\vec{\mathbf{D}}} + \kappa\underline{\vec{\mathbf{E}}} + \underline{\vec{\mathbf{J}}_0} \qquad (31)$$

$$\mathbf{div}\,\underline{\vec{\mathbf{D}}} = \rho \qquad (32)$$

$$\mathbf{div}\,\underline{\vec{\mathbf{B}}} = \mathbf{0}. \qquad (33)$$

The system (30) - (33) leads to

$$\mathbf{div}\,((i\omega\varepsilon + \kappa)\underline{\vec{\mathbf{E}}}) = -\mathbf{div}\,(\underline{\vec{\mathbf{J}}_0}). \qquad (34)$$

The electric field $\underline{\vec{\mathbf{E}}}$ may be described as the gradient of a scalar potential because of (30). Note that this is a complex potential:

$$\underline{\vec{\mathbf{E}}} = -\mathbf{grad}\,\underline{\varphi}. \qquad (35)$$

Thus the governing equation for the electric scalar potential becomes:

$$\mathbf{div}\,((i\omega\varepsilon + \kappa)\,\mathbf{grad}\,\underline{\varphi}) = \mathbf{div}\,(\underline{\vec{\mathbf{J}}_0}). \qquad (36)$$

2.2 Numerical Simulation with FIT

The application of FIT leads to the following equivalence between continuous and discretized equations

$$\begin{aligned} \mathrm{div}((i\omega\varepsilon+\kappa)\,\mathbf{grad}\,\underline{\varphi}) &= \mathrm{div}(\underline{\vec{J}_0}) \quad (37)\\ \Longleftrightarrow\ \tilde{\mathbf{S}}(\mathbf{D}_\kappa+i\omega\mathbf{D}_\varepsilon)\tilde{\mathbf{S}}^{\mathbf{T}}\underline{\Phi}_{\mathbf{E}} &= \tilde{\mathbf{S}}\underline{\mathbf{j}}_0. \quad (38)\end{aligned}$$

Introducing the notation

$$\mathbf{A}_\kappa := \tilde{\mathbf{S}}\mathbf{D}_\kappa\tilde{\mathbf{S}}^{\mathbf{T}},\ \mathbf{A}_\varepsilon := \tilde{\mathbf{S}}\mathbf{D}_\varepsilon\tilde{\mathbf{S}}^{\mathbf{T}},\ \underline{\mathbf{p}}_0 := \tilde{\mathbf{S}}\underline{\mathbf{j}}_0. \quad (39)$$

the governing complex linear system for the field problem becomes

$$(\mathbf{A}_\kappa+i\omega\mathbf{A}_\varepsilon)\underline{\Phi}_{\mathbf{E}} = \underline{\mathbf{p}}_0. \quad (40)$$

Comparison with electrostatics and stationary currents shows that the real part of the complex symmetric matrix $\mathbf{A} = \mathbf{A}_\kappa + i\omega\mathbf{A}_\varepsilon$ is just the matrix $\mathbf{A}_\kappa$ for stationary currents and the imaginary part is the matrix $\mathbf{A}_\varepsilon$ of electrostatics, scaled with the frequency ω. $\mathbf{A}$ is a sparse $(N \times N)$ matrix connecting neighboring potentials. Electro-quasistatics is now implemented in the MAFIA [14] static solver S.

3 Waveguide Boundaries in the Frequency Domain

An important issue in numerical electromagnetics is the computation of reflection and transmission coefficients of structures terminated by infinitely long waveguides. In [5] an algorithm is described to simulate such waveguide boundaries using MAFIA's [14] time domain solver T3.

In the following a variant of this method will be derived to be used within the frequency domain module for driven problems W3 (cf. [10]).

Transforming Maxwell's Grid Equations into the frequency domain yields

$$\begin{aligned} \mathbf{Ce} &= -i\omega\mathbf{b} \quad (41)\\ \tilde{\mathbf{C}}\mathbf{D}_\mu^{-1}\mathbf{b} &= i\omega\mathbf{D}_\varepsilon\mathbf{e}+\mathbf{j} \quad (42)\end{aligned}$$

Inserting (41) in (42) we get the so-called *curl-curl-equation*

$$\tilde{\mathbf{C}}\mathbf{D}_\mu^{-1}\mathbf{Ce}-\omega^2\mathbf{D}_\varepsilon\mathbf{e} = -i\omega\mathbf{j}, \quad (43)$$

corresponding to the analytical form

$$\mathbf{curl}\ \mu^{-1}\mathbf{curl}\ \vec{\mathbf{E}}-\omega^2\epsilon\vec{\mathbf{E}} = -i\omega\vec{\mathbf{J}}. \quad (44)$$

The system matrix of (43)

$$\mathbf{A}_1 = \tilde{\mathbf{C}}\mathbf{D}_\mu^{-1}\mathbf{C}-\omega^2\mathbf{D}_\epsilon$$

is complex symmetric in the general lossy case and real symmetric in the loss-free case having real material coefficients ϵ and μ.

$\mathbf{A}_1$ is a large sparse $(3N_P \times 3N_P)$ matrix, connecting only neighbouring components of the solution vector $\mathbf{e}$. Thus the introduction of any boundary condition only requires the correcбion of those entries of $\mathbf{A}_1$, which concern the tangential $\vec{E}$-components at the boundary plane, as demonstrated in Fig. 2.

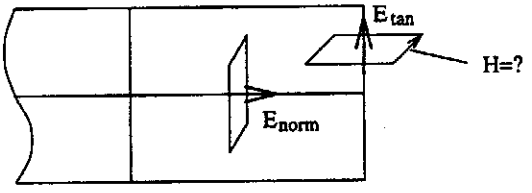

Figure 2: Introducing boundary conditions: Only the curl around E_{tan} has to be corrected, whereas the curl around E_{norm} lies completely inside the grid.

In the following we consider the waveguide termination shown in Fig. 3.

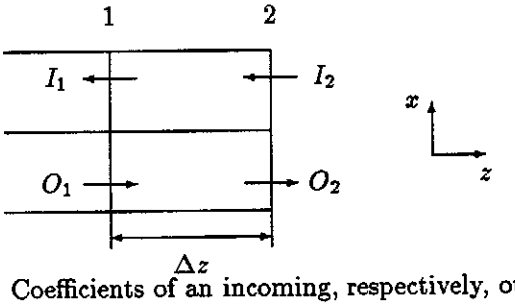

Figure 3: Coefficients of an incoming, respectively, outgoing wave at a waveguide boundary.

To obtain the tangential $\vec{E}$-field at the boundary plane 2, a modal expansion at plane 1 is performed, one grid step in front of the termination. The eigenmodes in a waveguide satisfy the analytical orthogonality relation

$$\int\int_A (\vec{E}_i(x,y)\times H_j^*(x,y))\cdot dA = \delta_{ij},$$

or in gridspace

$$(\mathbf{e}_i,\mathbf{h}_j) := \mathbf{e}_i\mathbf{K}\mathbf{h}_j = \delta_{ij}$$

with a topological matrix $\mathbf{K}$ (cf.[5]). The indexed vectors $\mathbf{e}_i$ and $\mathbf{h}_j$ refer to the 2-dimensional modes in the waveguide, and are expanded to full 3D-length where necessary.

The tangential field in plane 1 can be written as a superposition of all these modes

$$\mathbf{e}(x, y, z_1) = \sum_1^\infty a_i \mathbf{e}_i(x, y), \tag{45}$$

where the a_i are given in gridspace by

$$a_i = (\mathbf{e}(z_1), \mathbf{h}_i).$$

Each of these coefficients a_i can be split up into two parts propagating along $\pm z$-direction, named I_1 and O_1 as shown in Fig. 3.

Assuming $k_z(\omega)$ to be the propagation constant of the waveguide mode, the coefficients at planes 1 and 2 satisfy

$$\begin{aligned} I_1 = e^{-ik_z\Delta z} I_2 \quad &, \quad O_2 = e^{-ik_z\Delta z} O_1 \\ a_1 = I_1 + O_1 \quad &, \quad a_2 = I_2 + O_2 \end{aligned} \tag{46}$$

From this we get the following algorithm to obtain the tangential $\vec{E}$-components at plane 2:

1. Compute the discrete 2D-eigenmodes (including their propagation constants) of the infinitely long waveguide using MAFIA's eigenmode solver E.
2. Perform a modal expansion of the tangential electric field at plane 1, yielding coefficients a_i for a number of modes.
3. Compute $a_2 = I_2 + O_2$ at plane 2, where I_2, representing a wave coming from outside the structure, is known a priori. From (46) we have
$$a_2 = I_2(1 - e^{-2ik_z\Delta z}) + a_1 e^{-ik_z\Delta z}.$$
4. Compute the tangential electrical field at plane 2 from (45).

Finally this algorithm has to be transformed in a matrix-equation conforming to (43). The tangential field at the boundary plane is (considering only one eigenmode)

$$\begin{aligned} \mathbf{e}(z_2) &= a_2 \mathbf{e}_i \\ &= [I_2(1 - e^{-2ik_z\Delta z}) + a_1 e^{-ik_z\Delta z}]\, \mathbf{e}_i \end{aligned}$$

with

$$\begin{aligned} a_1 \mathbf{e}_i &= (\mathbf{e}(z_1), \mathbf{h}_i)\, \mathbf{e}_i \\ &= (\mathbf{e}_i \mathbf{h}_i^T \mathbf{K})\, \mathbf{e}(z_1). \end{aligned}$$

Including this formula in the matrix-equation (43), we get a new linear system

$$\mathbf{A}_2 \mathbf{e} = \mathbf{b}_2,$$

with the extended system matrix

$$\mathbf{A}_2 = \mathbf{A}_1 + \omega^2 \mathbf{D}_\epsilon e^{-ik_{z,i}\Delta z} \sum_i (\mathbf{e}_i \mathbf{h}_i^T \mathbf{K}), \tag{47}$$

where the summation has to be performed over all modes considered in the modal expansion.

The excitation by the incoming wave(s) with coefficients $I_{2,i}$ is included in the right hand side

$$\mathbf{b}_2 = -i\omega \mathbf{j} - \omega^2 \mathbf{D}_\epsilon \sum_i I_{2,i}(1 - e^{-2ik_{z,i}\Delta z}) \mathbf{e}_i.$$

The new system matrix is

- *complex* due to the propagating term $e^{-ik_{z,i}\Delta z}$ and
- *nonsymmetric* due to the fact, that the modal expansion is performed in plane 1, but its results are applied in plane 2.

The final computation of the desired S-parameters is quite a simple task, since the amplitudes of the outgoing waves O_2 at the boundary plane (respectively their power O_2^2) just have to be normalized to the power of the exciting mode (I_2^2).

4 Solution of the Linear Problems

To obtain the solution vectors of the discretized problems it is necessary to solve a large sparse indefinite system of complex-valued linear equations. With the calculation of three-dimensional structures the dimension N of the system matrix is usually in the order of magnitude $10^3 - 10^7$ which necessitates the application of iterative methods in the solution process. An important class of iterative methods available for this task are the so-called Krylov subspace methods in which

$$x_n \in x_0 + K_m \tag{48}$$

holds for the iterative approximates x_n to the true solution $A^{-1}b$, where one has a Krylov subspace

$$K_m = K_m(A, r_0) := \{v \in \mathbf{R}^N | v = \sum_{i=0}^{m-1} c_i A^i r_0\} \tag{49}$$

with $r_0 = b - Ax_0$. This includes the original CG (Conjugate gradient) method by Hestenes and Stiefel [11] and its descendants to which one often refers to as conjugate gradient type methods.

The subject of Krylov subspace methods is still an exciting active field of ongoing research and the number of recent publications in this field documents the

interest with which these methods for the solution of non-Hermitian linear systems of equations have been received by computer scientists and numerical engineers.

Unfortunately Krylov subspace methods for non-Hermitian systems are not sufficiently robust to be applied as blackbox solvers. There are examples of system matrices for which each of the methods presented here will fail to reach a prescribed level of accuracy or fails to even converge at all. Not all of these examples are of academic nature and thus a careful testing of the different methods available is mandatory in order to see which solver is most suited for a given problem. The range of methods tested here does not include algorithms like the well-established GMRES method by Saad and Schulz [19], the GMERR method by Weiss [34] or the just recently published GMBACK method by Kasenally [13]. To be competitive these methods generally require, even in restarted versions, the storage of a large number of basis vectors of length N. Thus, as memory efficiency is here an important consideration for three-dimensional problems, these methods cannot be recommended. Also not considered are methods based on the normalized equation such as CGNR and the CGNE method by Craig [3]. The normalization of the system matrix results also in a squaring of the condition number which may severely affect the iteration process. The expected slow speed of convergence did not encourage their application right from the start.

Both the system matrices of equation (40) arising in electro-quasistatics and the discretized eddy-current problem without the new waveguide boundaries yield symmetric systems of complex linear equations ($A = A^T \neq A^H$) which then have to be solved.

A solution method which has already proven its feasibility [10] for this process is the COCG (Conjugate Orthogonal Conjugate Gradient) algorithm by van der Vorst and Melissen [26]. This method is effectively a symmetric variant of the complex BiCG algorithm (Bi-Conjugate Gradient) of Jacobs [12]. In the BiCG method the iterates fullfil a Petrov-Galerkin condition

$$b - Ax_n \perp L_n \text{ with } x_n \in x_0 + K_n, \qquad (50)$$

where one has Krylov subspaces $K_n = K_n(A, r_0)$ with $r_0 = b - Ax_0$ and $L_n = K_n(A^H, \tilde{r}_0)$, where $\tilde{r}_0$ is an additional non-trivial starting vector. The choice of $\tilde{r}_0 = \bar{r}_0$, which is the conjugate complex of the starting residual r_0, in the complex symmetric case allows the simplification of the calculation of the factors α_n and β_n in the BiCG algorithm, since an additional expensive matrix vector multiplication with the conjugate-transpose system matrix A^H is no longer needed. In the following the inner product is defined as $\langle x, y\rangle := y^H x = \bar{y}^T x$, where $\bar{y}$ is the conjugate complex of the vector y. The vectorial formulation of the COCG algorithm reads:

COCG algorithm (without preconditioning)
Let $A \in \mathbf{C}^{N\times N}, A = A^T, b \in \mathbf{C}^N, x_0 \in \mathbf{C}^N$
Choose $x_0 \in \mathbf{C}^N$
$p_0 = r_0 = b - Ax_0$; $\rho_0 = \langle r_0, \bar{r}_0\rangle$;
For $n = 0, 1, \ldots$ **do:**
$\sigma_n = \langle Ap_n, \bar{p}_n\rangle$; $\alpha_n = \rho_n/\sigma_n$;
$x_{n+1} = x_n + \alpha_n p_n$;
$r_{n+1} = r_n - \alpha_n Ap_n$;
If x_{n+1} is accurate enough: **Stop.**
$\rho_{n+1} = \langle r_{n+1}, \bar{r}_{n+1}\rangle$; $\beta_n = \rho_{n+1}/\rho_n$;
$p_{n+1} = r_{n+1} + \beta_n p_n$;
End.

As long as the system matrix is complex symmetric this method may be suspected to be the best choice since there is only one matrix vector multiplication to be performed at each iteration step.

In practice however, for reasons of stability, this problem sometimes has to be tackled by other, more expensive modern CG-type methods which where mainly developed for more general systems of complex linear equations. Their application becomes essentially necessary with the introduction of the new waveguide boundaries to the discrete time harmonic equation, due to the non-symmmetric system matrix. Here the BiCG method can be applied. It is also the basis for more modern methods which will be presented in the following text:

BiCG algorithm (without preconditioning)
Choose x_0; $r_0 = b - Ax_0$;
$p_{-1} = \tilde{p}_{-1} = 0$; $\rho_{-1} = 1$;
Choose $\tilde{r}_0$, such that $\rho_0 = \langle r_0, \tilde{r}_0\rangle \neq 0$;
For $n = 0, 1, \ldots$ **do:**
$\beta_n = \rho_n/\rho_{n-1}$;
$p_n = r_n + \beta_n p_n$;
$\tilde{p}_n = \tilde{r}_n + \bar{\beta}_n \tilde{p}_n$;
$v_n = Ap_n$;
$\sigma_n = \langle v_n, \tilde{r}_n\rangle$; $\alpha_n = \rho_n/\sigma_n$;
$x_{n+1} = x_n + \alpha_n p_n$;
If x_{n+1} is accurate enough: **Stop.**
$r_{n+1} = r_n - \alpha_n v_n$;
$\tilde{r}_{n+1} = \tilde{r}_n - \bar{\alpha}_n A^H \tilde{p}_n$;
$\rho_{n+1} = \langle r_{n+1}, \tilde{r}_{n+1}\rangle$;
End.

According to Sonneveld [25] the calculation of the vectors p_n and r_n can be considered as the construction of so-called BiCG polynomials of degree n $\psi_n, \phi_n \in \Pi_n$ (where $\Pi_n = \{q | q(t) = \sum_{i=0}^{n} a_i t, q(0) = 1, a_i \in \mathbf{R}\}$), which fulfil the corresponding three-term recurrence for p_n and r_n :

$$r_n = \phi_n^{\text{BiCG}}(A) r_0, \quad p_n = \psi_n^{\text{BiCG}}(A) r_0.$$

His idea for the CGS (Conjugate Gradient Squared) algorithm was to exploit an eventually existing contraction

property of the BiCG polynomials, which are also applied for the calculation of the so-called pseudo-residuals $\tilde{r}_n$ and pseudo-search directions $\tilde{p}_n$ in the BiCG algorithm. Implicitly the CGS algorithm then calculates

$$r_n = (\phi_n^{\text{BiCG}})^2(A)r_0, \quad p_n = (\psi_n^{\text{BiCG}})^2(A)r_0,$$

without requiring the construction of $\tilde{r}_n$ and $\tilde{p}_n$ which would necessitate a matrix vector multiplication with the conjugate-transpose of A as in the original BiCG method. It has iterates

$$x_n \in x_0 + K_{2n}(A, r_0).$$

The CGS algorithm theoretically converges if BiCG does and is usually faster in a lot of practical applications.

CGS algorithm (without preconditioning)
Choose x_0; $r_0 = b - Ax_0$;
$q_0 = p_{-1} = 0$; $\rho_{-1} = 1$;
Choose $\tilde{r}_0$, such that $\rho_0 = \langle r_0, \tilde{r}_0 \rangle \neq 0$;
For $n = 0, 1, \ldots$ **do:**
$\beta_n = \rho_n / \rho_{n-1}$;
$u_n = r_n + \beta_n q_n$;
$p_n = u_n + \beta_n(q_n + \beta_n p_{n-1})$;
$v_n = Ap_n$;
$\sigma_n = \langle v_n, \tilde{r}_0 \rangle$; $\alpha_n = \rho_n / \sigma_n$;
$q_{n+1} = u_n - \alpha_n v_n$;
$x_{n+1} = x_n + \alpha_n(u_n + q_{n+1})$;
If x_{n+1} is accurate enough: **Stop.**
$r_{n+1} = r_n - \alpha_n A(u_n + q_{n+1})$;
$\rho_{n+1} = \langle r_{n+1}, \tilde{r}_0 \rangle$;
End.

The squaring of the BiCG polynomials is characteristic of the CGS method and results in either an amplification of any existing contraction property of the polynomials or an increase of the residual norms depending on the choice of the start vector r_0.

This cause for the often observed irregular convergence behavior may result in numerical cancellation which can severely affect the stability of these methods. Several new stabilized methods have been developed to overcome this effect. Fokkema, Sleijpen and van der Vorst [21] developed generalized variants of the CGS method and probably its closest relative is the CGS2 method. Here one has

$$r_n = \tilde{\phi}_n(A)\phi(A)r_0$$

for a nearby BiCG polynomial $\tilde{\phi}_n$ based on some vector $\tilde{s}$ instead of $\tilde{r}$. Another variant of a generalized CG method is the BiCGSTAB (Bi-Conjugate Gradient stabilized) method [27] by van der Vorst. For BiCGSTAB he proposed to define the residuals r_n by

$$r_n = \pi_n(A)\phi_n^{\text{BiCG}}(A)r_0,$$

$\pi_n \in \Pi_n$ defined as a product of n 1-step MR-polynomials (Minimal Residual), i.e., n degree one polynomials:

$$\pi_n(t) = (1 - \omega_1 t)(1 - \omega_2 t)\ldots(1 - \omega_n t).$$

The ω_i are chosen to minimize the Euclidean norm of r_n :

$$\|r_n(\omega_n)\| = \min_{\omega \in \mathbf{R}} \|(1 - \omega A)\pi_{n-1}(A)\phi_n^{\text{BiCG}}(A)r_0\|_2.$$

The BiCGSTAB method is the combination of a BiCG polynomial followed by an GMRES(1) minimization step and thus usually yields smoother convergence curves than CGS. However, stagnation or even breakdown may occur if the ω_i are close to zero. To overcome this effect Gutknecht [9] proposed the usage of a 2-step MR-polynomial in every second iteration step. A generalization of this idea was given by Sleijpen and Fokkema [20] with the introduction of l-step MR-polynomials which led to the more efficient BiCGstab(l) algorithm with

$$\pi_n = \chi_m \chi_{m-1} \cdots \chi_0,$$

where $n = ml + l$, $\chi_i \in \Pi_l$ and χ_m minimizing

$$\|\chi_m(A)\pi_{n-l}(A)\phi_n^{\text{BiCG}}(A)r_0\|_2.$$

This method can essentially be considered as a combination of BiCG and GMRES(l) and it holds

$$x_k = x_{lm} \in x_0 + K_{2ml}(A, r_0).$$

Thus for $l = 1$ this method coincides with the original BiCGSTAB algorithm. We also tested an implementation with $l = 2$. Even here stagnation may occur, if its GMRES(2) part stagnates.

BiCGstab(l) algorithm (without preconditioning)
Start:
Choose $\mathbf{x}_0, \tilde{r}_0$; $\mathbf{r}_0 = b - A\mathbf{x}_0$;
$\mathbf{p}_{-1} = 0$; $\rho_0 = 1$, $\alpha = 0$, $\omega = 1$;
For $n = 0, l, 2l, \ldots$ **do:**
$p_0 = \mathbf{p}_{n-1}$; $r_0 = \mathbf{r}_n$; $x_0 = \mathbf{x}_n$
$\rho = -\omega\rho_0$;
For $j = 0, \cdots, l-1$ do:
$\rho_1 = \langle r_j, \tilde{r}_0 \rangle$; $\beta = \alpha\rho_1/\rho_0$; $\rho_0 = \rho_1$;
For $i = 0, \cdots, j$ do:
$p_i = r_i - \beta p_i$
End;
$p_{j+1} = Ap_j$; $\gamma = \langle p_{j+1}, \tilde{r}_0 \rangle$; $\alpha = \rho_0/\gamma$;
For $i = 0, \cdots, j$ do:
$r_i = r_i - \alpha p_{i+1}$
End;
$r_{j+1} = Ar_j$; $x_0 = x_0 + \alpha p_0$;
End;

For $j = 1, \cdots, l$ do:
  For $i = 1, \cdots, j-1$ do:
    $\tau_{ij} = (1/\sigma_i)\langle r_j, r_i\rangle$;
    $r_j = r_j - \tau_{ij} r_i$
  End;
  $\sigma_j = \langle r_j, r_j\rangle$; $\gamma_j' = (1/\sigma_j)\langle r_0, r_j\rangle$;
End;
$\gamma_l = \gamma_l'$; $\omega = \gamma_l$;
For $j = l-1, \ldots, 1$:
  $\gamma_j = \gamma_j' - \sum_{i=j+1}^{l} \tau_{ji}\gamma_i$;
End;
For $j = 1, \ldots, l-1$:
  $\gamma_j'' = \gamma_{j+1} + \sum_{i=j+1}^{l-1} \tau_{ji}\gamma_{i+1}$;
End;
  $x_0 = x_0 + \gamma_1 r_0$; $r_0 = r_0 - \gamma_l' r_l$; $p_0 = p_0 - \gamma_l p_l$;
For $j = 1, \cdots, l-1$:
  $p_0 = p_0 - \gamma_j p_j$; $x_0 = x_0 + \gamma_j'' r_j$; $r_0 = r_0 - \gamma_j' r_j$;
End;
$\mathbf{u}_{n+l-1} = u_0$; $\mathbf{r}_{n+l} = r_0$; $\mathbf{x}_{n+l} = x_0$;
If $\mathbf{x}_{n+l}$ is accurate enough: **Stop.**
End.

The TFQMR (Transpose-free Quasi-Minimal Residual) algorithm by Freund [7] is closely related to the CGS algorithm (cf. [7],[36]). The quasi-minimal residual approach was used first in the BiCG-based QMR algorithm by Freund and Nachtigal [8] and yields smoother convergence curves. It usually exhibits a performance similar to CGS and CGS2. The vectorial TFQMR algorithm reads as:

TFQMR algorithm (without preconditioning)
Choose x_0;
$w_1 = y_1 = r_0 = b - Ax_0$; $v_0 = Ay_1$;
$d_0 = 0$; $\tau = \|r_0\|$; $\vartheta_0 = 0$; $\eta_0 = 0$;
Choose $\tilde{r}_0$, such that $\rho_0 = \langle r_0, \tilde{r}_0\rangle \neq 0$;
For $n = 1, 2, \ldots$ **do:**
$\sigma_{n-1} = \langle v_{n-1}, \tilde{r}_0\rangle$; $\alpha_{n-1} = \rho_{n-1}/\sigma_{n-1}$;
$y_{2n} = y_{2n-1} - \alpha_{n-1} v_{n-1}$;
  For $m = 2n-1, \ldots, 2n$ **do:**
    $w_{m+1} = w_m - \alpha_{n-1} A y_m$;
    $\vartheta_m = \|w_{m+1}\|/\tau_{m-1}$; $c_m = 1/\sqrt{1+\vartheta_m^2}$;
    $\tau_m = \tau_{m-1}\vartheta_m c_m$; $\eta_m = c_m^2 \alpha_{n-1}$;
    $d_m = y_m + \left(\vartheta_{m-1}^2 \eta_{m-1}/\alpha_{n-1}\right) d_{m-1}$;
    $x_m = x_{m-1} + \eta_m d_m$;
    If x_m is accurate enough: **Stop.**
$\rho_n = \langle w_{2n+1}, \tilde{r}_0\rangle$; $\beta_n = \rho_n/\rho_{n-1}$;
$y_{2n+1} = w_{2n+1} + \beta_n y_{2n}$;
$v_n = Ay_{2n+1} + \beta_n(Ay_{2n} + \beta_n v_{n-1})$;
End.

Note that for this version of the TFQMR algorithm only an upper bound is given for the residual norm. All the methods presented here belong to the family of biconjugate gradient-based methods.

The performance of all Krylov subspace methods strongly depends on the spectrum of the system matrix. Thus a preconditioning of the system matrix is almost always mandatory to improve the distribution of its eigenvalues in the complex plane. This is usually performed by solving a system

$$P_1^{-1} A P_2^{-1} (P_2 x) = P_1^{-1} b \tag{51}$$

instead of the original system $Ax = b$. The better the matrix $M = P_1 P_2$ approximates A, the better one may expect the associated acceleration methods to perform. A common choice for M is an incomplete approximation of A or, adapted to the requirements of specialized computer hardware, a matrix $s(A)$,where s is a suitably chosen low-degree polynomial. For a good survey on this subject see [1], [17] and [16]. The theoretical effects of preconditioning on systems of linear equations may be considered to be quite well understood if the system matrix is an M-matrix. For more general systems of linear equations they are not completely understood and so the preconditioning of non-Hermitian complex matrices is still based to a large extent on numerical experience. For a visualization of the effects of preconditioners on the spectra of a number of test matrices see [15]. For the solution of the electro-quasistatic system (40) an SSOR and an $\mathrm{MIC}_\omega(0)$ preconditioner [1] was applied. Both preconditioning methods have a positive effect on the spectrum of the complex symmetric linear system and yield a considerable reduction in the number of iterations required in the tested CG-type methods.

For the nonsymmetric system of complex linear equations arising from the discrete time harmonic equations with waveguide boundaries a different approach was taken. A memory efficient SSOR left-preconditioning was applied, which had already been implemented for the symmetric case with the preconditioning matrix

$$M = \left(\frac{1}{\tilde{\omega}}\Delta - L\right)\left(\frac{1}{\tilde{\omega}}\Delta\right)^{-1}\left(\frac{1}{\tilde{\omega}}\Delta - U\right), \tag{52}$$

where Δ is the diagonal, L the strictly lower and U the strictly upper part of the symmetric part

$$\mathbf{A}_1 = \tilde{\mathbf{C}}\mathbf{D}_\mu^{-1}\mathbf{C} - \omega^2 \mathbf{D}_\epsilon \tag{53}$$

of the nonsymmetric system matrix A_2 and $\tilde{\omega}$ is a suitably chosen acceleration parameter. A common choice is $\tilde{\omega} = 1$, since there is usually only a small sensitivity of the preconditioning process to this parameter. We may refer to this approach as a *Partial*-SSOR preconditioning.

A very similar approach for this problem was investigated by Yserentant [35] for indefinite symmetric system matrices as they arise in the discretization of Helmholtz-type elliptic equations. He applied a matrix B arising

from the symmetric, positive definite part of such an indefinite matrix A as a split-preconditioner to the whole system and gave estimates on the spectrum of this preconditioned system. Their consequences for Krylov subspace methods were also pointed out.

A priori considerations on the feasibility of this ansatz were confirmed for our applications with the expected nice performance at the solution of very large systems of equations (cf. Example 4 and 5).

5 Numerical Results

For the linear systems of equations of the previous sections the methods presented in the previous chapter were coded and tested. Here a small number of different test calculations will be given. Some of them are of rather academic interest whereas others (in general the larger problems) correspond to computer simulations of real world problems. All the calculations have been performed on a SUN Microsystems computer in double precision.

5.1 Example Calculations for Electro-Quasistatics:

Example 1:

Fig. 4 shows a typical convergence history for a simple square plate capacitor model with side length 8 cm and a thickness of 3 cm. Its dielectric material was assumed to have a relative permittivity of $\varepsilon_r = 3$ and a conductivity of $\kappa = 10^{-6}$ S/m. A voltage gradient of 15 kV/cm was assumed at a frequency f of 50 Hz. The dimension of the complex symmetric linear system to be solved was 45177.

Example 2:

As an instance for a more realistic application a cylindrical insulator of solid epoxy resin is simulated. The model is a 30 mm long piece of the cylindrical insulator with some droplets on its surface. It was discretized with a $57 \times 57 \times 73$ grid yielding a system of 237177 complex unknowns. The epoxy resin has a relative permittivity of $\epsilon_r = 4$, the droplets have $\epsilon_r = 81$ and a conductivity of about $\kappa = 10^{-6}$ S/m. A frequency f of 50 Hz and a voltage gradient of 5 kV/cm is assumed. Fig. 5 shows a first result for the real part of the electric field when only seven droplets are taken.

Simulations for high voltage insulators often were based on electrostatic calculations [2]. Since the electrostatic approach does not take into account the current density and the displacement current, it is obvious that a systematic error is inherent to this model. Fig. 6 gives a comparison of the longitudinal electric field along the insulator from one corona to the other. This path crosses some of the droplets, each of which causing a large peak in the field intensity. The electrostatic model shows large discrepancies in these areas of interest. Consequently, the electro-quasistatic model should be preferred for simulations of high voltage insulators.

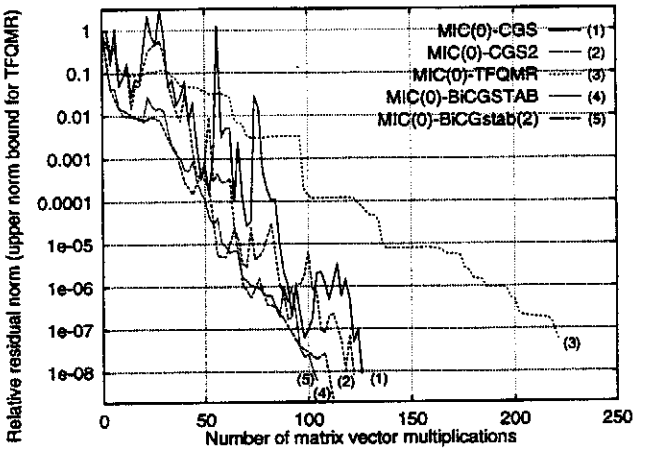

Figure 4: Example 1: Convergence history for an example with 45177 grid points and MIC(0)-left preconditioning with $\omega = -0.5$.

Fig. 7 shows the isometric lines of the real part of the electro-quasistatic potential when the droplets are placed in one row along the insulator.

5.2 Example Calculations for Time Harmonic Problems Including Waveguide Boundaries:

Example 3:

The first small test example of this subsection for time harmonic problems including waveguide boundaries is only of academic interest. A filament strip is included inside a rectangular domain with a waveguide boundary condition at one side (cf. Fig. 8). The domain is discretized with a $4 \times 3 \times 4$ grid and yields an non-symmetric system of complex linear equations with 144 unknowns. For the application of the *Partial*-SSOR left-preconditioning to the system matrix the convergence of all tested CG-type methods did deteriorate (cf. Fig. 10 and 11). This had to be expected since the number of gridpoints belonging to the waveguide boundary was considerable, compared to the whole number of gridpoints. Note the stagnation of the preconditioned and the non-preconditioned BiCGSTAB algorithm even for this small example.

Fig. 9 shows the distribution of the eigenvalues of

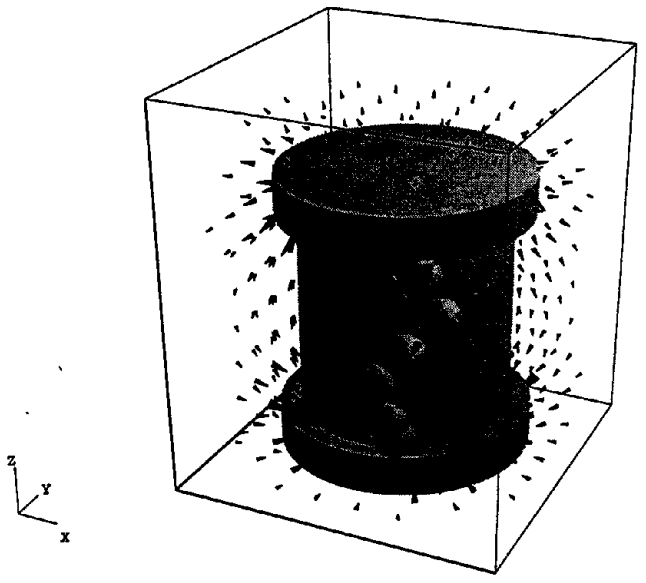

Figure 5: Example 2: Arrow plot of the real part of the electric field for an insulator with some water drops.

the system matrix with and without the new waveguide boundaries.

Example 4:

In this test example the S-parameters of a 3 db waveguide coupler (Fig. 12) are calculated. It was discretized with a $52 \times 2 \times 128$ grid yielding a system of 40704 complex linear equations. For this larger problem the application of the *Partial*-SSOR-preconditioning to the system significantly reduced the number of iterations required in the solution process (Fig. 15). Note that the CGS-related methods CGS2 and TFQMR exhibited the same rate of convergence as CGS (Fig. 14).

As a result, Fig. 16 shows the reflection-coefficient S_{11} for three frequencies, compared to the result of a time domain calculation (cf. [5]). The agreement between both algorithms is excellent.

Example 5:

The structure shown in Fig.17 is a piece of a chip showing two micro strip ports and two thin wires connecting the strips with resistive blocks on the material. The resistive blocks have a conductivity $\kappa = 13000\text{S/m}$, while the substrate has permittivity, $\epsilon = 9.0$. The geometrical extensions are about $700\mu m \times 300\mu m$. The problem here was to determine the cross talk from one wire to the other at a frequency of 10, resp. 40 Ghz. This structure was discretized with a $71 \times 20 \times 85$ grid, which required the solution of a non-symmetric linear system of equations with 362100 complex unknowns. The stabilized convergence behavior of the PSSOR preconditioned TFQMR method allowed this system to be solved with about 3000 iterations in 17.46 h on a SUN Sparc 20

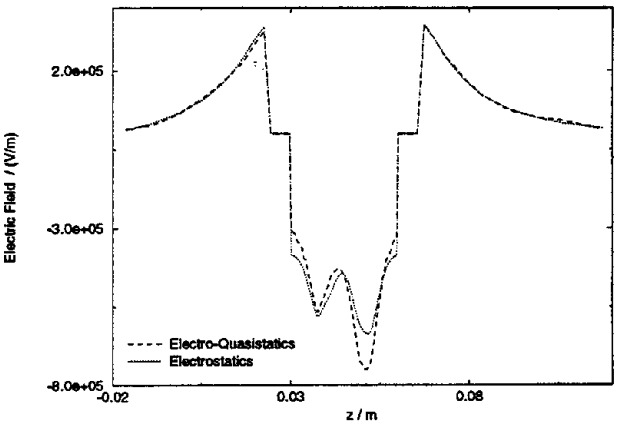

Figure 6: The dashed curve with the most distinct minimum shows the z-component of $\mathrm{Re}(\vec{E})$ as a function of z corresponding to an electro-quasistatic calculation, the dotted curve with the z-component of $\vec{E}$ results from a electrostatic calculation.

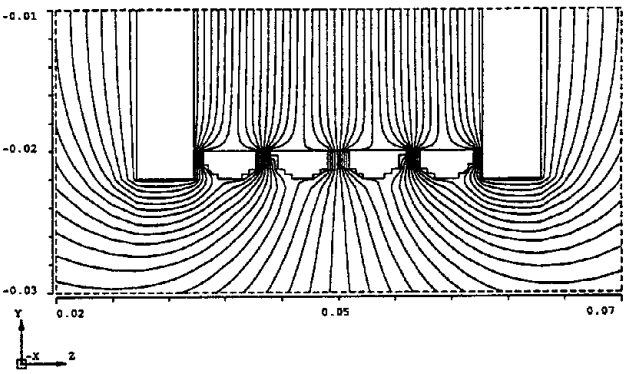

Figure 7: Contourplot of the real part of the potential $Re(\Phi_E)$ in the cutting plane of four droplets in a row along the z-axis.

computer to a prescribed level of accuracy. The non-preconditioned BiCG method did not converge for this problem, as shown in Fig. 18. The S-parameters obtained again agree excellently with the solution of the time domain calculations.

6 Conclusions and further work

Several modern Krylov subspace type methods were implemented to solve the discretized complex linear system of equations which arise from the two areas of computer simulation of electromagnetic fields: First we presented the electro-quasistatics with its complex symmetric linear systems of equations. In most cases they can be efficiently solved using the COCG algorithm, whereas the

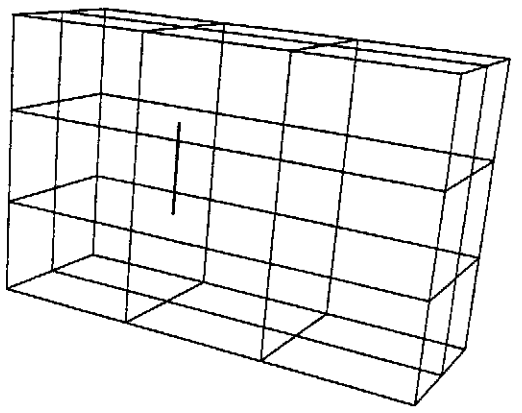

Figure 8: Example 3: $4 \times 3 \times 4$ grid of the small academic example.

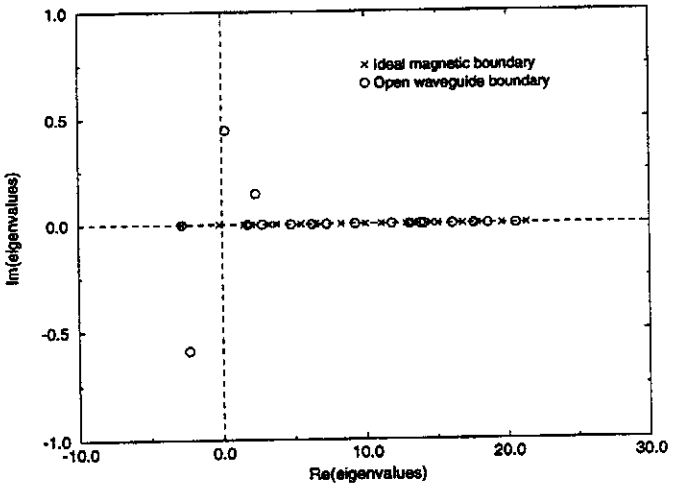

Figure 9: Example 3: Distribution of the eigenvalues of the system matrices. The nonsymmetric matrix arising from the formulation including waveguide boundaries has also eigenvalues with non-vanishing imaginary part.

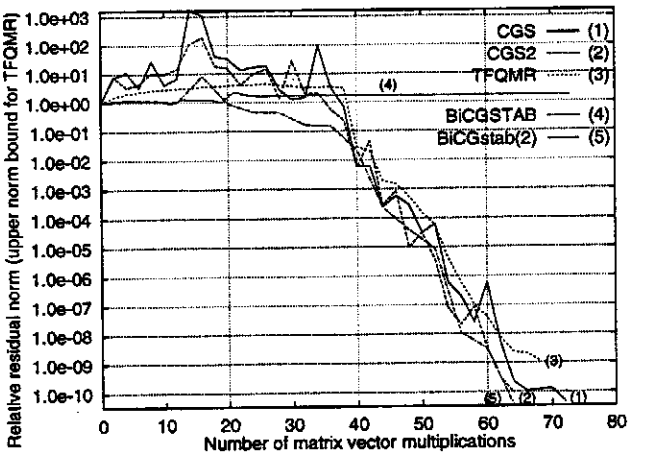

Figure 10: Example 3: Convergence curves of the tested solvers without preconditioning.

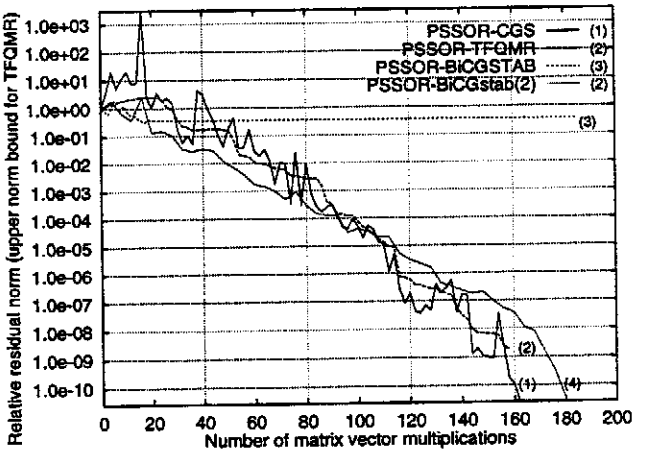

Figure 11: Example 3: Convergence curves of the tested solvers with preconditioning. The convergence rate is here worse than for the non-preconditioned system due to the small number of mesh points.

more expensive MIC_ω-preconditioned stabilized methods BiCGSTAB and BiCGstab(2) can here be considered to be a feasible choice to circumvent any BiCG-related irregular convergence behavior of the COCG method.

The COCG method has already been successfully applied for the solution of complex symmetric linear systems in 3D eddy current computations with the frequency domain solver module W3 of MAFIA [10]. These systems of equations became non-symmetric after the introduction of a new type of boundary condition for waveguides. It was shown that only BiCG, CGS and their stabilized variants CGS2 and TFQMR perform appropriately in their solution. With BiCG converging, we may assume the BiCGSTAB method to suffer here from the stagnation of its GMRES(1) part. It stagnated here even for the PSSOR preconditioned system. In the BiCGstab(2) method the better residual minimization property of its GMRES(2) part seemed to remove the stagnation problem, but still the overall performance was not competitive. Further work will aim at the improvement of the convergence properties of the BiCGSTAB methods including recent results of Sleijpen and van der Vorst [23], [22], [24].

The very next step has to be an improvement in terms of an even more efficient preconditioning of this system. A direct approach will surely be the inclusion of the yet omitted nonsymmetric part of the system matrix into the SSOR preconditioning matrix, though we might expect only a small improvement to the overall iteration process for large problems. More hope is set in the implementation of preconditioners which are based on a sophisticated incomplete factorization such as (M)ILU(k) [1] or ILUT(k, ϵ) [18], their variants without fill-in could

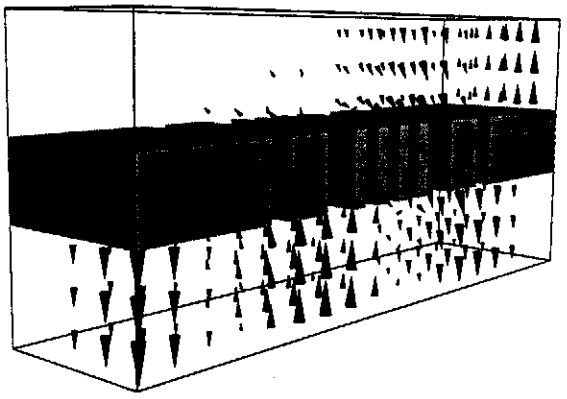

Figure 12: Example 4: Real part of the electrical field Re(E) in a 3 db waveguide coupler.

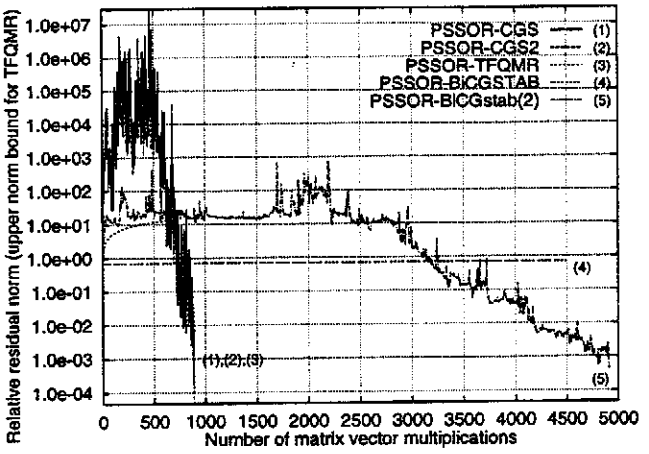

Figure 13: Example 4: Convergence curves of different preconditioned solvers. The CGS-related solvers CGS2 and TFQMR exhibit almost the same rate of convergence, while BiCGSTAB completely fails and BiCGstab(2) takes about five times the amount of work to reach the prescribed level of accuracy for the relative residual.

be coded in an efficient Eisenstat implementation [6].

7 Acknowledgements

We would like to acknowledge the helpful suggestions and comments from Mrs. Suzan Wipf and Dr. Eugene Tomer. We are indebted to Prof. Henk van der Vorst, whose review of an earlier version of this paper helped improving it in many ways.

References

[1] O. Axelsson. A survey of preconditioned iterative methods for linear systems of algebraic equations. *BIT*, 16:166–187, 1985.

[2] Oliver Claus and Hans-Joachim Klös, 1994. Private Communications.

[3] E. J. Craig. The n-step iteration procedures. *Math. Phys.*, (34):64–73, 1955.

[4] Michael Dehler. *Numerische Lösung der Maxwellschen Gleichungen auf kreiszylindrischen Gittern.* PhD thesis, Technische Hochschule Darmstadt, 1993.

[5] Martin Dohlus. *Ein Beitrag zur numerischen Berechnung elektromagnetischer Felder im Zeitbereich.* PhD thesis, Technische Hochschule Darmstadt, 1992.

[6] Stanley C. Eisenstat. Efficient implementation of a class of preconditioned conjugate gradient methods. *SIAM Sci. Stat. Comput.*, 2(1):1–4, March 1981.

[7] Roland W. Freund. A transpose-free quasi-minimal residual algorithm for non-Hermitian linear systems. *SIAM J. Sci. Comput.*, 14(2):470–482, March 1993.

[8] Roland W. Freund and Noel M. Nachtigal. QMR: A quasi-minimal residual method for non-Hermitian matrices. *Numer.Math.*, 60:315–339, 1991.

[9] Martin H. Gutknecht. Variants of BICGSTAB for matrices with complex spectrum. *SIAM J. Sci. Stat.*, 14(5):1020–1033, September 1993.

[10] Peter Hahne. *Zur Numerischen Feldberechnung Zeitharmonischer Elektromagnetischer Felder.* PhD thesis, Technische Hochschule Darmstadt, 1992.

[11] M. R. Hestenes and E. Stiefel. Methods of conjugate gradients for solving linear systems. *J. Res. Nat. Bur. Standards*, 49:409–436, 1952.

[12] D. A. H. Jacobs. *The Exploitation of Sparsity by Iterative Methods.* Sparse matrices and their Uses. I. S. Duff, Springer, 1981. pp. 191-222.

[13] Ebrahim M. Kasenally. GMBACK: A generalised minimum backward error algorithm for nonsymmetric linear systems. *SIAM J. Sci. Comput.*, 16(3):698–719, May 1995.

[14] The Mafia collaboration. *User's Guide MAFIA Version 3.x.* CST GmbH, Lauteschlägerstr.38, D-64289 Darmstadt.

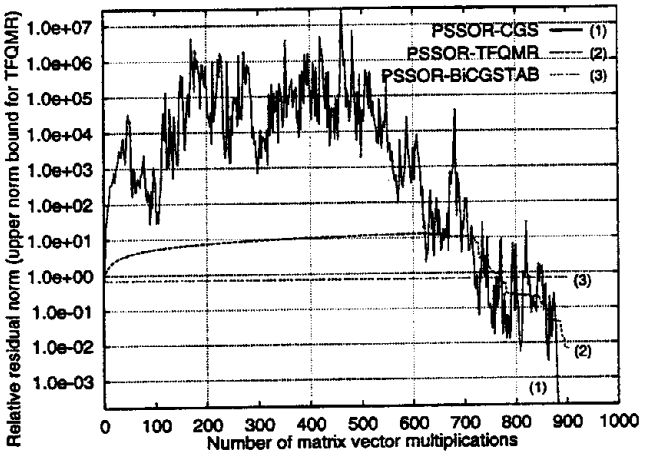

Figure 14: Example 4: Convergence curves of TFQMR, CGS, CGS2 and BiCGSTAB with PSSOR preconditioning. BiCGSTAB stagnates almost immediately after a few steps.

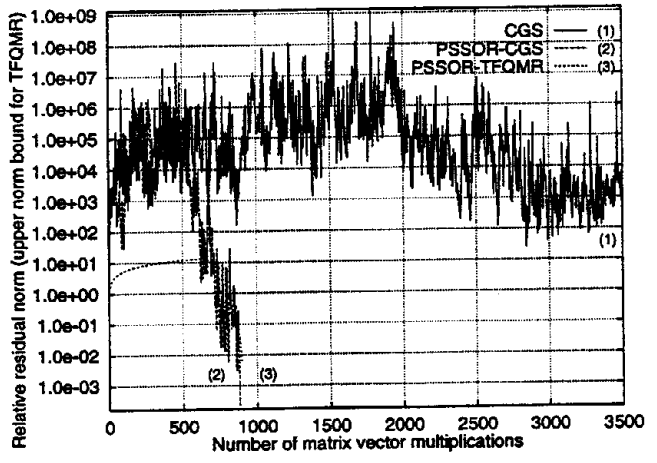

Figure 15: Example 4: Convergence curves of PSSOR preconditioned CGS and TFQMR methods versus the CGS method without preconditioning.

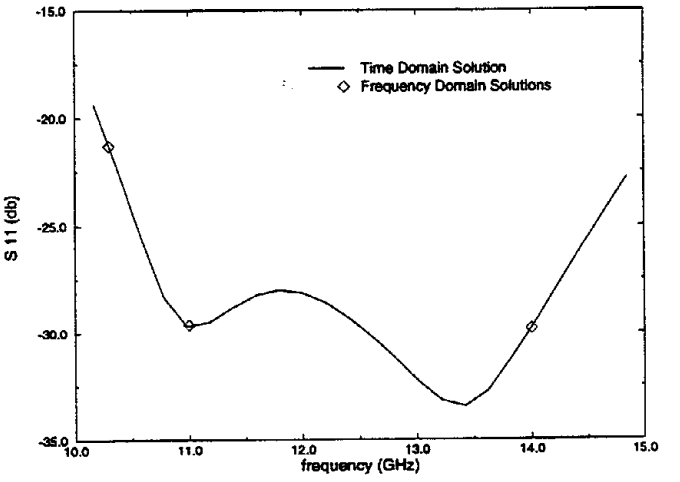

Figure 16: Example 4: Reflection coefficient S_{11} of the 3 db waveguide coupler. The results from the frequency domain computation show excellent agreement with the time domain solution.

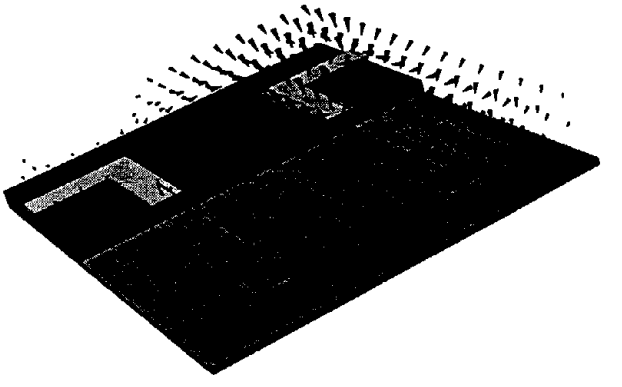

Figure 17: Example 5: Cross talk of the electrical field (real part Re(E), logarithmically scaled) at a frequency of 10 GHz.

[15] Ulrike Meier Yang. Preconditioned conjugate gradient methods for nonsymmetric linear systems. Research Report 1210, CSRD, University of Illinois at Urbana Champaign, July 1994.

[16] Yousef Saad. Preconditioning techniques for nonsymmetric and indefinite linear systems. *Journal of Computational and Applied Mathematics*, (24):89–105, 1988.

[17] Yousef Saad. Krylov subspace methods on supercomputers. *SIAM J. Sci. Stat. Comput.*, 10(6):1200–1232, 1989.

[18] Yousef Saad. ILUT: a dual treshold incomplete LU factorization. *Numerical Linear Algebra with Applications*, 1(4):387–402, 1994.

[19] Yousef Saad and Martin H. Schultz. GMRES: A generalised minimal residual method for solving nonsymmetric linear systems. *SIAM J. Sci. Stat. Comput.*, 7:856–869, 1986.

[20] Gerard L. G. Sleijpen and Diederik R. Fokkema. BICGstab(l) for linear equations involving unsymmetric matrices with complex spectrum. *Electronic Transactions on Numerical Analysis*, 1:11–32, September 1993.

[21] Gerard L. G. Sleijpen, Diederik R. Fokkema, and Henk A. van der Vorst. Generalized Conjugate Gradient Squared. University Utrecht, Department of Mathematics, Preprint No. 851, May 1994.

[22] Gerard L. G. Sleijpen and Henk A. van der Vorst. Reliable updated residuals in hybrid Bi-CG meth-

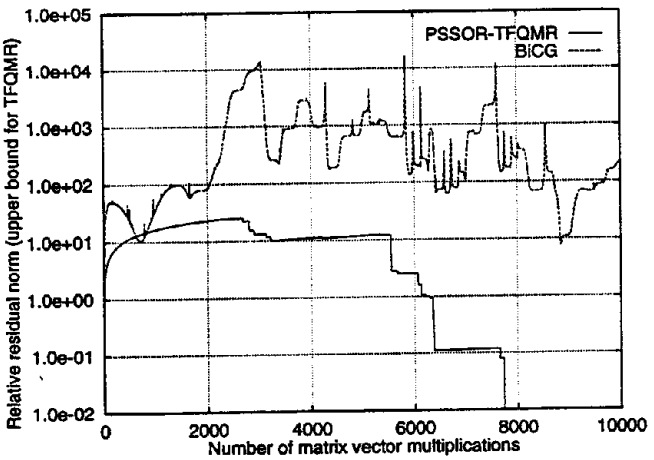

Figure 18: Example 5: Convergence curves of PSSOR preconditioned TFQMR method versus the non-preconditioned BiCG method.

ods. University Utrecht, Department of Mathematics, Preprint No. 886, to appear in Computing, November 1994.

[23] Gerard L. G. Sleijpen and Henk A. van der Vorst. Maintaining convergence properties of BiCGstab methods in finite precision arithmetic. *Numerical Algorithms*, 10:203–223, 1995.

[24] Gerard L. G. Sleijpen and Henk A. van der Vorst. An overview of approaches for the stable computation of hybrid Bi-CG methods. University Utrecht, Department of Mathematics, Preprint No. 908, to appear in Appl. Numer. Math., March 1995.

[25] Peter Sonneveld. CGS, a fast Lanczos-type solver for nonsymmetric linear systems. *SIAM J. Sci. Stat. Comput.*, 10(1):36–52, November 1989.

[26] H. A. van der Vorst and J.B.M. Melissen. A Petrow-Galerkin type method for solving Ax=b, where A is symmetric complex. *IEEE Trans.Mag.*, 26(2):706–708, 1990.

[27] Henk A. van der Vorst. Bi-CGStab: A fast and smoothly converging variant of Bi-CG for the solution of nonsymmetric linear systems. *SIAM J. Sci. Stat. Comput.*, 2(13):631–644, 1992.

[28] Ursula van Rienen and Thomas Weiland. Triangular discretization method for the evaluation of RF-fields in cylindrically symmetric cavities. *Particle Accelerators*, 20:239–267, 1987.

[29] Thomas Weiland. A discretization method for the solution of Maxwell's equations for six-component fields. *Electronics and Communcations AEÜ*, 31:116, 1977.

[30] Thomas Weiland. A numerical method for the solution of the eigenvalue problem of longitudinally homogeneous waveguides. *Electronics and Communcations AEÜ*, 31:308, 1977.

[31] Thomas Weiland. Lossy waveguides with arbitrary boundary contour and distribution of material. *Electronics and Communcations AEÜ*, 33:170, 1979.

[32] Thomas Weiland. On the numerical solution of Maxwellian equations and applications. *Particle Accelerators*, 15:245–291, 1984.

[33] Thomas Weiland. On the unique numerical solution of Maxwellian eigenvalue problems in three dimensions. *Particle Accelerators*, 17:227–242, 1985.

[34] Rüdiger Weiss. Error-minimizing Krylov subspace methods. *SIAM J. Sci. Comput.*, 15(3):511–527, May 1994.

[35] Harry Yserentant. Preconditioning indefinite discretization matrices. *Numer. Math.*, 54:719–735, 1988.

[36] L. Zhuo and F. Walker. Residual smoothing techniques for iterative methods. *SIAM J. Sci. Comput.*, 15(2):297–312, March 1994.